JOURNAL OF APPLIED ELECTROCHEMISTRY 17 (1987) 165–173

The impedance of alkaline manganese cells and their relationship to cell performance. I. Interpretation of the basic impedance spectrum

R. BARNARD, L. M. BAUGH*, C. F. RANDELL

Ever Ready Limited, Technical Division, Tanfield Lea, Stanley, Co. Durham, UK

Received 11 March 1986

The impedance characteristics of undischarged alkaline manganese cells of various sizes (LR20, LR6 and LR03) have been investigated over the frequency range 100 kHz to 1 mHz. Specially constructed reference electrode probes have been inserted into the cells in two basic positions such as to obtain a complete analysis of the contribution to the total impedance from the individual cell components. It is shown that the impedance of standard cells is determined by the cathode–can assembly, the anode–separator impedance being negligible by comparison. The cathode–can impedance is further resolved into two components. Firstly, a component due to a nickel oxide layer present on the surface of the nickel-plated steel can. This takes the form of a high frequency semicircle in the complex plane. Secondly, a component due to the cathode itself (manganese dioxide + graphite mixture) which takes the form of a higher frequency semicircle and a low-frequency straight line of slope $\sim 32°$. The latter is interpreted in terms of porous electrode behaviour involving slow proton diffusion in the solid state. Some evidence for a porous–planar transition has also been obtained at a critical frequency of ~ 3 mHz.

1. Introduction

Alkaline manganese cells occupy the premium position within the primary cell volume market. This position is dependent upon their excellent high-rate performance and good storage capabilities. There is, however, a need to understand in more detail the fundamental electrochemical processes which determine the superior performance characteristics of these cells in order that further improvements might be implemented. While it is possible to study the electrodes and components in isolation in model experiments using conventional electrochemical techniques, considerable advantages can accrue if an *in situ* method of study is adopted, since the results obtained have more direct consequences in terms of complete battery behaviour. The impedance method is one such technique which can be applied, and an extensive survey of the impedance characteristics of various primary cells, including the alkaline manganese system [1, 2], has been made by Karunathilaka *et al.* These authors have published reveiws for the case of the primary aqueous systems [3, 4]. A general conclusion from this work was that in the undischarged state the impedance of all the systems studied, namely Leclanché, alkaline manganese and zinc–mercuric oxide, is dominated by that of the zinc electrode. Confirmation of this result has been made in the case of Leclanché [5] and zinc chloride Leclanché cells [6].

The present work is concerned with a reappraisal of the interpretation of the impedance of alkaline manganese cells. Specially constructed reference electrode probes have been inserted into pilot scale production cells in order to obtain a complete analysis of the contribution to the impedance from individual cell components. This method yields unambiguously the major contributor(s) without making any assumptions concerning a model for either the cell impedance or that of the individual electrode reactions. The relationship of the measured impedance parameters to battery performance will be discussed in subsequent papers.

* *Present address*: BNF Metals Technology Centre, Grove Laboratories, Denchworth Road, Wantage, Oxon, UK.

0021–891X/87 $03.00 + .12

Table 1. Electrode configurations and relationship to the impedance of individual cell components

Electrode configuration	*Number of electrodes employed*	*Location of voltage measurement*	*Impedance component determined*
A	2	Cathode–can/anode cap	Whole cell
B	3	1. Cathode–can/Ref. 1	Can + cathode
C	3	2. Cathode–can/Ref. 2	Can
D	3	3. Anode cap/Ref. 2	Anode + separator + cathode
E	3	4. Anode cap/Ref. 1	Anode + separator
F	4	Ref. 1/Ref. 2	Cathode

The resistance of electrolyte contributes to the impedance of all components except the can.

2. Experimental details

The cells employed in the present investigation were generally pilot scale production LR20, LR6 or LR03 size, although the LR6 cells of some competitors have also been examined.

The impedance measurements were made via a galvanostatic method in which a sinusoidal current perturbation was imposed between the cathode can and anode cap while the voltage response was monitored according to Table 1. The essence of the investigation involved the use of reference electrodes in two positions designated reference 1 and reference 2 as shown schematically in Fig. 1. In position 1 the reference electrode was placed adjacent to the separator on the cathode side and in position 2 it was placed just inside the can. The reference electrodes were zinc wires (1 mm) sheathed in irradiated poly(olefin) shrink tubing. By suitable choice of working and counter electrode combinations, various electrode configurations were set up which resulted in a complete breakdown of the impedance of the individual cell components as illustrated in Table 1. The electrode configurations are designated A to F. In electrode configuration A, connections to the impedance measuring circuit were made via the cathode can and anode cap only and no reference electrode was employed. This resulted in the impedance of the whole cell being determined. In electrode configurations B to E a *single* reference electrode was employed either in position 1 or 2, the exact impedance component determined being dependent upon choice of working–counter electrode connections. In configuration F *two* reference electrodes were employed, one in position 1 and the other in position 2. The impedance component determined was that of the cathode only.

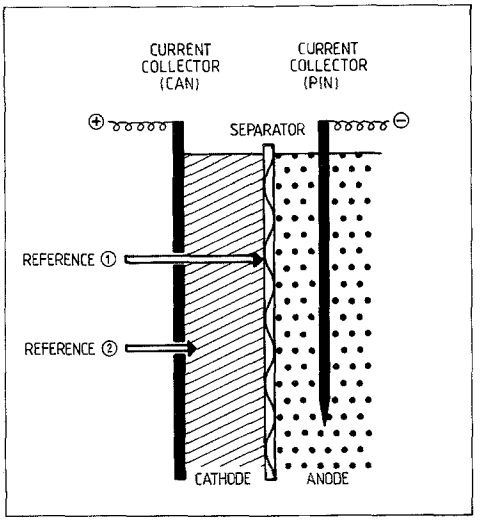

Fig. 1. Schematic diagram of part of an alkaline manganese cell showing the basic reference electrode positions 1 and 2.

Two different methods were employed for determining the impedance depending upon the frequency of measurement. In both methods, however, the a.c. signal source was a Brookdeal 9471 or 9473. At high frequencies (100 kHz to 1 Hz) the in-phase and out-of-phase components of the a.c. current and voltage were measured using a Brookdeal 9503 Precision Lock-in Amplifier. The choice of frequency, data acquisition and impedance calculation was under partial computer control using a Commodore CBM 4032 microcomputer. At low frequencies (0.5 Hz to 1 mHz) the a.c. current and voltage were analysed using a 3D (Digital Design and Development) 12 bit A–D convertor. The data

acquisition and changing of frequency together with the impedance calculation was carried out under full control by the Commodore CBM 4032 microcomputer. A full description of the use of the microcomputer in determining the impedance will be published in due course [7].

3. Results and discussion

3.1. *General impedance characteristics and isolation of the major impedance contributors*

Fig. 2(a–e) illustrates the impedance characteristics of a standard undischarged LR20 cell obtained with the working–reference electrode configurations in positions A to E, respectively, as indicated in Table 1. It is clear that the cell impedance is determined by that of the cathode–can assembly and not by the anode–separator system which is negligible by comparison (cf. Fig. 2b, e). This conclusion is at variance with that of Karunathilaka *et al.* [1, 2]. From the comparisons shown in Fig. 2 it is also clear that the semicircle observed in the frequency range 20 kHz to 300 Hz is generated predominantly at the cathode–can interface and that the low frequency straight line of slope $\sim 30°$ is generated by the cathode itself. That these two impedances do not interact in any way is demonstrated from the overall impedance behaviour (Fig. 2a, b) and from the fact that they can easily be separated (Fig. 2c, d). Thus the semicircle part of the impedance is not a charge-transfer resistance and parallel double layer capacitance due to the manganese dioxide electrode as might superficially be assumed. Consequently, the semicircle must be due to a resistance and capacitance associated with the nickel oxide film, which must always be present on the surface of the nickel-plated steel can, together with any contact resistance–capacitance contributions within the cathode matrix close to the can wall or between the cathode and the nickel oxide layer. That this is a *general* result and not in any way peculiar to the particular cell under examination is demonstrated in Fig. 3 which shows a similar breakdown of the impedance for a commercially available competitor's LR20 cell. It is clear that any difference between Figs 2 and 3 is one of degree rather than kind. It is interesting to note that the

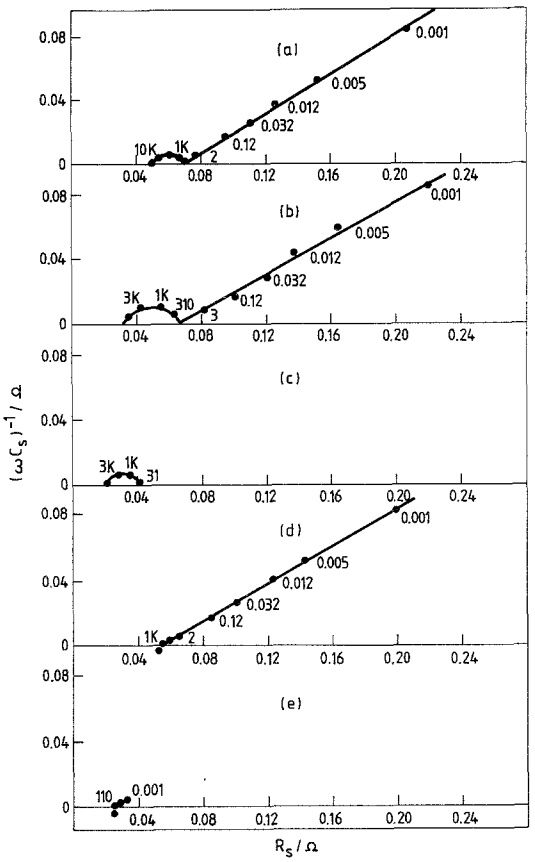

Fig. 2. Impedance characteristics for a standard LR20 pilot scale production cell obtained using electrode configurations A to E, respectively. (a) Impedance of the complete cell; (b) impedance of the cathode–can assembly; (c) impedance of the can; (d) impedance of the anode–separator system + cathode; (e) impedance of the anode–separator system.

low frequency anode impedance shown in Fig. 3d is a reasonably good straight line of slope 45° in agreement with that expected for a diffusion-controlled porous zinc electrode at frequencies below the porous–planar transition.

In order to confirm the general interpretation above, impedance measurements were made with cells constructed using cans which had been deliberately oxidized by heating in air at 600° C. This was expected to magnify the contribution to the impedance from the nickel oxide film whilst maintaining the other contributions approximately constant. The results are depicted in Fig. 4 where the electrode configurations are identical to those in Fig. 2. It can be seen that the only major change is an increase in the size of the

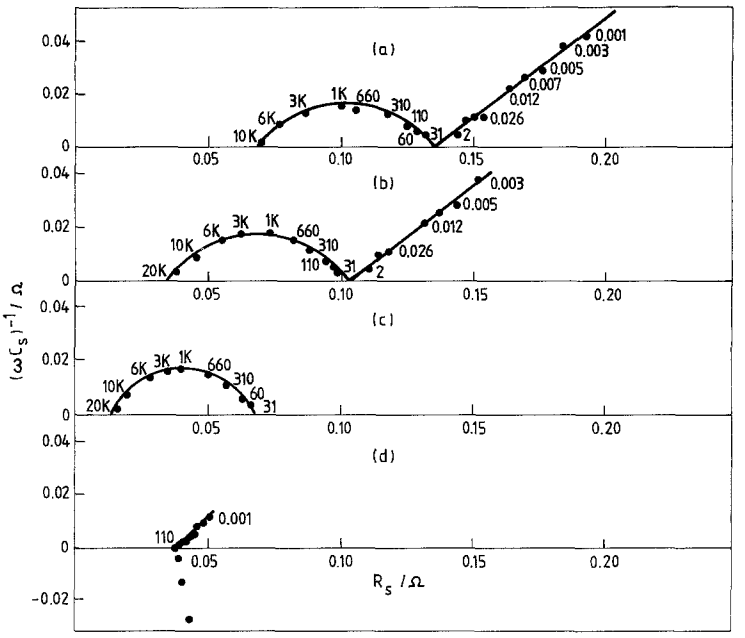

Fig. 3. Impedance characteristics for a competitor's commercially available LR20 cell obtained using electrode configurations A, B, C and E, respectively. (a) Impedance of the complete cell; (b) impedance of the cathode–can assembly; (c) impedance of the can; (d) impedance of the anode–separator system.

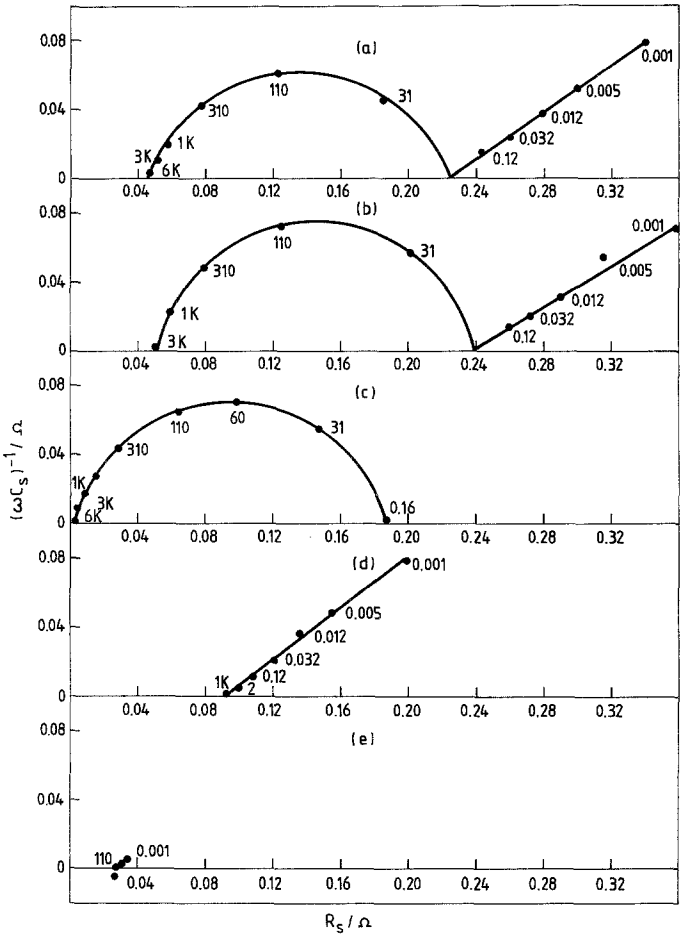

Fig. 4. Impedance characteristics for an LR20 size pilot scale production cell constructed using a can heated in air at 600° C. The electrode configurations are A to E, respectively, and are identical to those described in Fig. 2.

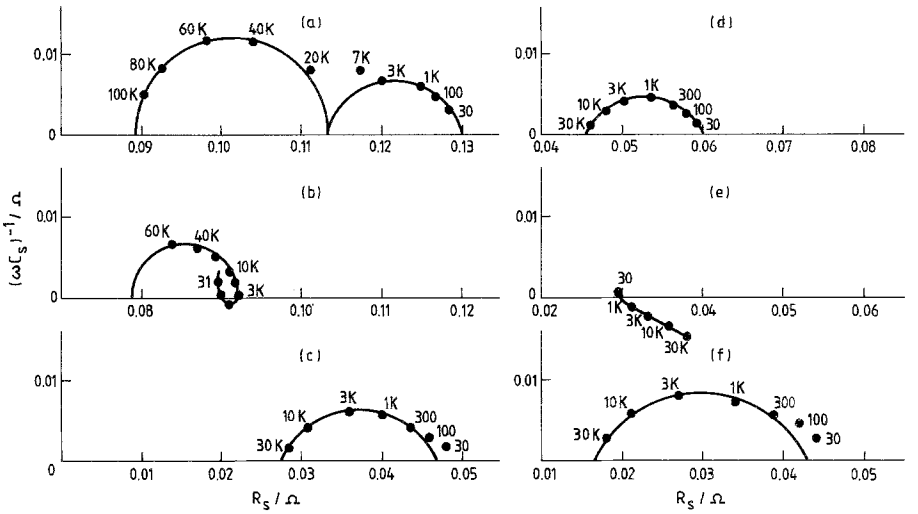

Fig. 5. High-frequency impedance characteristics for an LR20 pilot scale production cell containing a contact fault between the anode and anode current collector compared with standard impedance spectra. (a) Complete impedance spectrum of defective cell (electrode configuration A); (b) impedance of the anode–separator system for the defective cell (electrode configuration E); (c) impedance of the cathode–can assembly for the defective cell (electrode configuration C); (d) to (f) as (a) and (b) but for standard cell.

semicircle. The resistance of the thick oxide layer is $\sim 0.18\,\Omega$ and its capacitance ~ 0.015 F.

It can be concluded from the above that the major contributor to the impedance of typical undischarged alkaline manganese cells is the cathode–can assembly, the exact value being dependent upon the state of oxidation of the can. However, under certain circumstances the assumption that the impedance of the anode–separator system is negligible by comparison with that of the cathode–can assembly is invalid. Fig. 5 illustrates such a case. It compares the high frequency impedance characteristics for a standard LR20 cell with those of a cell which had poor contact between the anode pin and anode paste (see Fig. 1). The impedance behaviour of the whole cell, the anode–separator and cathode–can assemblies are shown individually (reference electrode position 1). The impedance characteristics for the cell containing the contact fault consists of two semicircles, the first at frequencies between 100 kHz and ~ 20 kHz and the second at frequencies between 3 kHz and 30 Hz. It is clear from the comparisons shown in Fig. 5 that the higher frequency semicircle is generated by the anode–separator system (Fig. 5b), while the lower frequency semicircle is due to the cathode–can assembly (Fig. 5c). The spectrum for the anode–separator system is interesting since it is very similar to that expected for a planar zinc electrode, including, for example, a low-frequency inductive component due to the presence of adsorbed intermediates [8]. A double-layer capacity of $\sim 60\,\mu F\,cm^{-2}$ can also be deduced (based on the surface area of the pin) which is of a very similar order to that expected for a rough planar zinc electrode at open circuit in concentrated alkaline solution [9]. Thus the abnormal impedance shown in Fig. 5a is due to the brass anode current collector which is in fact amalgamated and zinc plated as a result of contact with the anode and which acts as the major contributor to the impedance of the anode–separator system. This, as a result of the poor contact, effectively replaces the impedance of the porous zinc electrode which is small by comparison (cf. Fig. 5b, e). The parallel increase in the value of the high frequency intercept on the resistive axis from $0.030\,\Omega$ (Fig. 5e) to $0.078\,\Omega$ (Fig. 5b) suggests a change in the electrolyte resistance within the anode region due to the decreased interfacial electrode area. This change is mirrored by the high frequency intercept for the whole cell impedance (cf. Fig. 5a, d).

Fig. 5 indicates a further feature of the impedance characteristics of standard alkaline manganese cells upon which it is necessary to comment. At frequencies > 1 kHz the impedance

of the anode–separator system is inductive (Fig. 5e). This feature is also discernible in Figs 2e, 3d and 4e and may be a real effect or an artefact. Its absence from the impedance characteristics of the whole cell suggests the latter.

3.2. *Detailed impedance characteristics of the cathode–can assembly*

3.2.1. Separation of cathode and can contributions at high frequencies. As discussed in the previous section the high-frequency impedance characteristics of a *standard* alkaline manganese cell consists of a semicircle which is composed of two components, i.e. that due to the can oxide layer and that due to the cathode itself (or contact between the cathode matrix and the can oxide layer). Further experiments were directed towards the separation of these contributions. Two methods were employed. Firstly, subtraction of impedance values determined in experiments with electrode configuration C (Table 1) from the equivalent values determined with electrode configuration B. Fig. 6a shows the spectrum for an LR6 cell. That the spectrum contains contributions from two smaller semicircles is just discernible. Comparison of the cathode–can impedance (Fig. 6b) with the overall cell impedance again predicts that the anode–separator impedance is negligible. This is confirmed (Fig. 6c) where it can be seen that the latter is no more than a 'dot' on the resistive axis. Subtraction of the impedance of the can interface (Fig. 6d) from that of the cathode–can system as a whole (Fig. 6b) yields the impedance of the cathode alone (Fig. 6e). This exercise proves that the higher frequency semicircle ($f^* = 6$ kHz) is due to the cathode and the lower frequency semicircle ($f^* = 1$ kHz) is due to the can oxide. Clearly the two contributions are of a similar order. Fig. 7 shows an identical breakdown of the high-frequency impedance for a LR6 production cell from a competitor, where the initial demarcation of the impedance into two semicircles is by no means clear. This is due to the fact that the characteristic frequency, f^*, for the can is much higher (1 kHz) and therefore closer to that for the cathode (6 kHz), thus precluding any initial resolution. Nevertheless, a very similar final result is obtained from the detailed analysis.

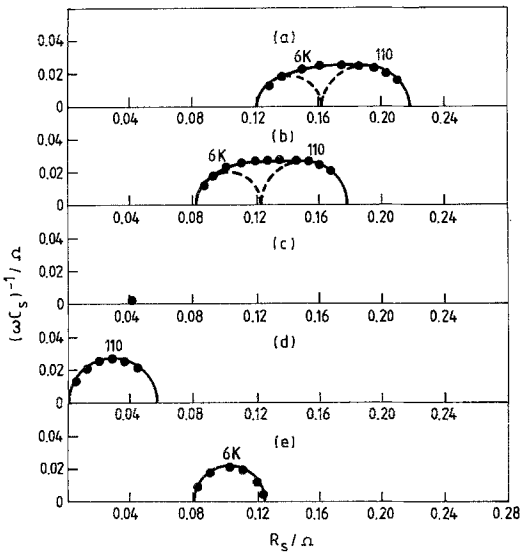

Fig. 6. High-frequency impedance spectra for a standard LR6 pilot scale production cell showing resolution into two semicircles attributable to the cathode (characteristic frequency 6 kHz) and the can (characteristic frequency 110 Hz). (a) Complete cell impedance (electrode configuration A); (b) impedance of the cathode–can assembly (electrode configuration B); (c) impedance of the anode–separator system (electrode configuration E); (d) impedance of the can (electrode configuration C); (e) impedance of the cathode determined by subtraction of (d) from (b). Dashed lines in (a) and (b) indicate position of (d) and (e) in the overall impedance spectrum.

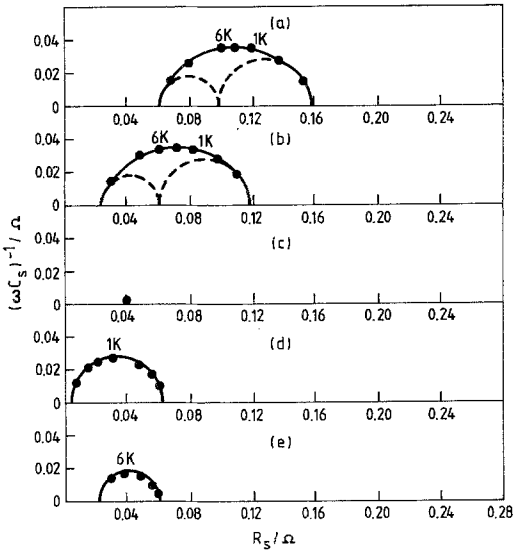

Fig. 7. High-frequency impedance spectra for a competitor's commercially available LR6 cell showing the same resolution into two semicircles as that described in Fig. 6.

A second approach was made in which the cathode impedance was determined *directly* without recourse to subtraction procedures. This involved electrode configuration F (Table 1). This is experimentally a much more difficult exercise since it involves the use of *two* reference electrodes in reasonably close proximity. Fig. 8 compares the high-frequency impedance spectra for an LR6 cell obtained using electrode configurations C, F and B when two reference electrodes are present within the cell. In contrast with the study shown in Fig. 7, the reference electrode in position 2 was studied somewhat further from the can surface. Thus, features in the impedance spectrum characteristic of the cathode also appear with electrode configuration C (Fig. 8a). Also, the high-frequency electrolyte resistance intercept is not zero as is normally the case when the reference electrode is very close to the can wall (cf. Figs 6d, 8a). Nevertheless, it is clear that the principle of the method is confirmed and the higher frequency cathode semicircle is isolated directly (Fig. 8b). The diameter of this semicircle is 0.04 Ω which is identical to that determined via the subtraction procedure (cf. Figs 6e, 7e, 8b).

While a high frequency cathode impedance component is clearly present in determining overall cell impedance characteristics in many instances, it is by no means clear at present how this arises. In principle, it is possible that the high-frequency cathode semicircle could be equated with a charge-transfer resistance and parallel double-layer capacity which should be observable if the reduction of manganese dioxide is only a quasi-reversible and not a completely reversible reaction. However, contact phenomena between graphite and MnO_2 particles or between the MnO_2 particles themselves may give rise to superficially similar results and further work is required to elucidate this point in more detail.

3.2.2. Low frequency cathode impedance characteristics. The low-frequency, straight line impedance spectrum of complete alkaline manganese cells (Figs 2, 3, 4) can be attributed exclusively to the cathode. The linearity of the complex impedance plot signifies that the manganese dioxide reduction process ($MnO_2 + H_2O + e \rightarrow MnOOH + OH^-$) occurs under diffusion-controlled conditions. It may be further supposed that this corresponds to the rate-determining diffusion of protons in the solid state. The slope of the complex impedance plot is close to 32° which is greater than that expected for a classical porous electrode of 22.5° [10] but smaller than that expected for a classical planar electrode of 45°. However, if it is assumed that the 32° portion of the plot does indeed correspond to porous electrode behaviour, then at sufficiently low frequencies a transition from porous to planar behaviour should occur when complete penetration of the porous cathode matrix by the a.c. signal occurs. Experiments were therefore carried out to test this hypothesis. Fig. 9 shows detailed low-frequency impedance spectra for three cell sizes: LR20, LR6 and LR03. It can be shown that the value of the high frequency intercept on the resistive axis and the value of the impedance (Z) at any frequency

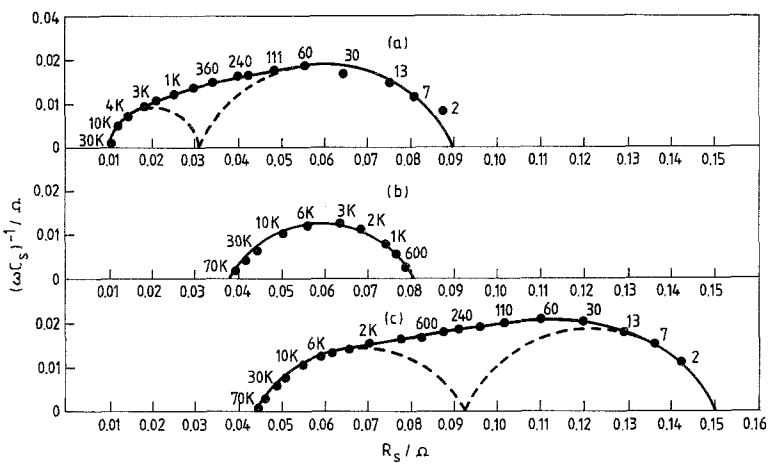

Fig. 8. High-frequency impedance spectra for an LR6 pilot scale production cell showing the cathode impedance determined by *direct* measurement compared with that of the can–cathode interface region and the complete cathode–can assembly. (a) Impedance of the can–cathode interface region (electrode configuration C); (b) impedance of the cathode only (electrode configuration F); (c) impedance of the complete cathode–can assembly (electrode configuration B).

vary in reasonably close agreement with that expected from the change in the geometrical area of the cathode rings in the different size cells. Evidence for a porous–planar transition at very low frequencies ($\lesssim 3$ mHz) is suggested in the case of the smaller LR6 and LR03 size cells. In the case of the LR20 cell, however, the much smaller impedance spectrum results in a situation where larger percentage errors are encountered in the measurements and hence there is a greater uncertainty regarding the impedance values, particularly at very low frequencies.

The porous–planar transition which is suggested from the data for LR6 and LR03 cells could occur at the critical frequency at which penetration of the entire porous structure (macropores and micropores) becomes complete. Laig-horstebrock has recently studied the potential response of cathode pellets having a very similar structure to those used in alkaline manganese cells [11]. He showed that in the early stages of the galvanostatic pulse ($i = 20$ mA) the potential follows a $t^{1/4}$ dependence, but this changes to a $t^{1/2}$ dependence at pulse lengths > 70 s. To explain these results a porous–planar model was presented. Conspicuously, the time required to penetrate the complete cathode matrix is of a very similar order to that expected from the critical frequency for the porous–planar transition determined in the present work. However, the conclusion of Laig-horstebrock that signal penetration occurs from one side of the cathode to the other in a direction parallel with the applied field (front to back face) does not appear to be borne out here, since a significant dependence of the critical frequency upon cathode *thickness* should be observed. Fig. 9 shows that the critical frequency is in fact independent of cathode thickness, since f^* is constant even though the thickness varies from 1.44 mm (LR03) to 2.13 mm (LR06). Further work is necessary to clarify the situation.

4. Conclusions

1. In addition to electrolyte resistance, the impedance of standard undischarged alkaline manganese cells is determined by the cathode–can assembly, the anode–separator impedance being negligible by comparison.

2. Only in exceptional circumstances, for example when there is very poor contact between the anode current collector and the anode material, does the anode–separator impedance become comparable with that of the cathode–can.

3. The cathode–can impedance is resolved into two components. Firstly, a contribution from the nickel oxide layer which is always present on the surface of the nickel-plated steel can. This takes the form of a high frequency

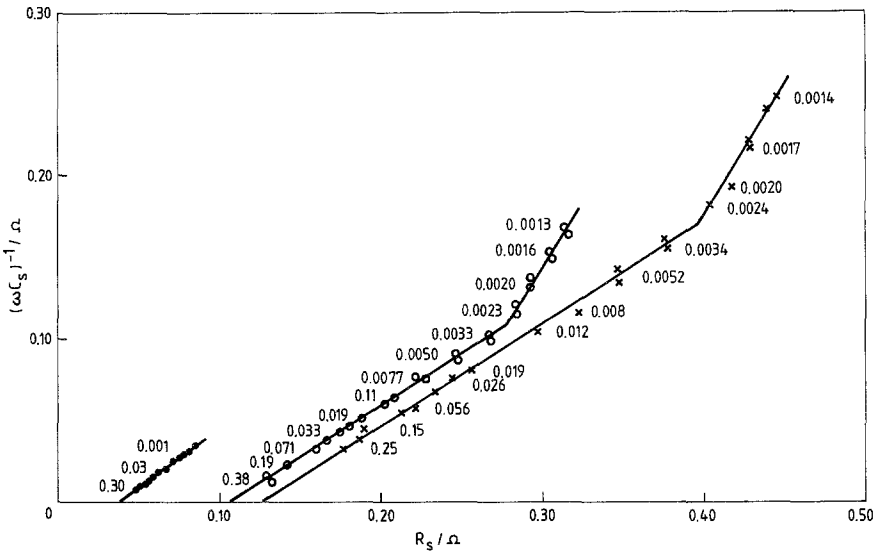

Fig. 9. Low-frequency impedance characteristics for LR20 (●), LR6 (○) and LR03 (×) pilot scale production cells.

semicircle in the complex plane. Secondly, a contribution from the cathode (manganese dioxide + graphite) material itself. This takes the form of a higher frequency semicircle and a low frequency straight line of slope $\sim 32°$.

4. The high-frequency cathode impedance may be equivalent to a charge-transfer resistance in parallel with a double-layer capacity, although this has not been proved. The low-frequency cathode impedance, however, is interpreted in terms of porous electrode behaviour involving slow proton diffusion in the solid state. At a critical frequency of ~ 3 mHz there is evidence of a transition from porous to planar behaviour when the whole wetted cathode matrix becomes electrochemically active.

5. It is predicted that the above impedance characteristics will have significant consequences regarding cell performance, particularly at high rates of discharge.

Acknowledgement

The authors wish to thank the Directors of British Ever Ready Limited for permission to publish this work.

References

[1] S. A. G. R. Karunathilaka, N. A. Hampson, R. Leek and T. J. Sinclair, *J. Appl. Electrochem.* **11** (1981) 365.
[2] *Idem, ibid.* **11** (1981) 715.
[3] S. A. G. R. Karunathilaka, N. A. Hampson and R. Leek, *Surf. Technol.* **13** (1981) 339.
[4] *Idem, J. Power Sources* **19** (1983) 205.
[5] L. M. Baugh and N. C. White, paper presented at 15th International Power Sources Symposium, Brighton, UK, 1986, and to be published in 'Power Sources 11' (edited by L. Pearce).
[6] *Idem*, to be published.
[7] C. F. Randell and N. C. White, to be published.
[8] R. D. Armstrong and N. F. Bell, *J. Electroanal. Chem.* **55** (1974) 201.
[9] L. M. Baugh, F. L. Tye and N. C. White, in 'Power Sources 9' (edited by J. Thomson), Academic Press, London (1983) p. 303.
[10] R. DeLevie, in 'Advances in Electrochemistry and Electrochemical Engineering', Vol. 6 (edited by P. Delahay and C. W. Tobias) Interscience, New York (1967) p. 329.
[11] H. Laig-horstebrock, *J. Electroanal. Chem.* **180** (1984) 599.